International Journal of Solids and Structures 202 (2020) 28–38

Contents lists available at ScienceDirect

International Journal of Solids and Structures

journal homepage: www.elsevier.com/locate/ijsolstr

Chirality in 2D Cosserat media related to stretch-micro-rotation coupling with links to granular micromechanics

Ivan Giorgio [a], Francesco dell'Isola [b], Anil Misra [c,*]

[a] Dipartimento di Ingegneria Civile, Edile-Architettura e Ambientale and MEMOCS, Università degli Studi dellAquila, Via Giovanni Gronchi 18 - Zona industriale di Pile, 67100 LAquila, Italy
[b] DISG Università di Roma La Sapienza, Italy
[c] Civil, Environmental and Architectural Engineering Department, University of Kansas, 1530 W. 15th Street, Learned Hall, Lawrence, KS 66045-7609, USA

ARTICLE INFO

Article history:
Received 17 February 2020
Received in revised form 20 April 2020
Accepted 3 June 2020
Available online 10 June 2020

Keywords:
Cosserat continua
Chiral media
Granular micromechanics
Stretch-micro-rotation coupling
Numerical modeling

ABSTRACT

Cosserat continuum model has attracted increasing interest for describing the mechanical behavior of microstructured solids. Existing formulation of Cosserat continuum model often overlooks chiral effects that arise from coupling between stretching deformations and the micro-rotation. Here, we introduce an extended Cosserat model that accounts for such a coupling. We discover the links of the extended model to the mechanics of granular materials and identify the continuum and grain-scale parameters that are the source of postulated chirality. The micro-rotation is shown to be related to the coupling of shear and normal responses of grain-pair interactions. The consequences of this chirality are then explicated with the aid of numerical examples. Through parametric studies we also demonstrate the possibility of measuring the effects of this type of chirality in experiments.

1. Introduction

In order to generalize the continuum model for deformable solids, Cosserat brothers introduced an additional, rotational, kinematic degree-of-freedom associated with every continuum material point (Cosserat and Cosserat, 1909). The ensuing theory and its further refinements or modifications are widely known as Cosserat continuum theory or micro-polar theory. Over the last century, this continuum theory has attracted wide-ranging attention and has been applied to explain certain size dependent phenomena exhibited by the so-called "micro-structured" solids (Altenbach et al., 2010; Berkache et al., 2019; Eremeyev and Pietraszkiewicz, 2016; Goda et al., 2012). However, the link between the continuum concept, and the kinematics and energetics at micro-structural scales, has been characteristically ignored or studied sporadically.

In this work, we focus attention upon the chiral behavior encoded within Cosserat continua. While chiral effects in Cosserat elasticity and higher-gradient media has been recognized (see for example (Lakes, 2001; Auffray et al., 2015), the micro-scale origins of this effect has been rarely explored. Only in recent years, with the advent of additive manufacturing and precision laser cutting, has there been attempt at realizing micro-structures that yield chiral micro-polar or higher-gradient continuum behavior (Frenzel et al., 2017; Ha et al., 2016; Reasa and Lakes, 2019; Poncelet et al., 2018; Chen et al., 2014; Liu and Hu, 2016). It is notable, however, that the key to rational design for achieving the desired behavior are predictive theories that link the macro-scale behavior to the micro-structural characteristics. Indeed, the pioneering work on 2nd and higher gradient theories leading to fabricated pantographic metamaterials are exemplar of such rational design (Seppecher et al., 2011; dell'Isola et al., 2018; Alibert et al., 2003; Abdoul-Anziz and Seppecher, 2018; dell'Isola et al., 2016; Turco et al., 2018; Andreaus et al., 2018; Barchiesi et al., 2019; Barchiesi and Placidi, 2017; Spagnuolo et al., 2019).

Towards that end, we investigate in this work the link between the 2D Cosserat chirality and mechanics of materials with granular microstructures, in which the relative movements between nearest grains, irrespective of where the deformation occurs, effectively describe the deformation occurring in the elastic grains. Such materials not only span the spectrum from naturally occurring highly consolidated dense solids formed of particulate precursors to confined packings of non-cohesive particles as discussed in (Nejadsadeghi and Misra, 2019), but also include materials that can be synthesized by specifying granular mechano-morphology. The response of these materials to imposed mechanical loads characteristically exhibits a range of complex behavior. By manipulating the microstructure and grain-interactions that can be realized

* Corresponding author.
E-mail address: amisra@ku.edu (A. Misra).

https://doi.org/10.1016/j.ijsolstr.2020.06.005
0020-7683/

using additive manufacturing, we believe it is possible to control their mechanical behavior. We have recently shown through granular micromechanics approach (GMA) based micromorphic continuum model (Nejadsadeghi and Misra, 2019; Misra and Poorsolhjouy, 2016) that particular types of grain-interactions can lead to emergent chiral behavior at the macro-scale (Misra et al., 2020). In particular, we used GMA to obtain closed-form expressions for elastic constants, which show that grain interactions that include coupling between normal and tangential deformations result in macro-scale chiral behavior for 2D isotropic granular media. We have then designed such a coupled grain-interaction for incorporation into 1D physical granular structure. The GMA predictions have been verified for 1D granular structure through a range of methods, including physical experiments, discrete granular models, enhanced Timeshenko beam model and finite element model of fully discretized structure (Misra et al., 2020; De Angelo et al., 2019). Here, we consider chirality of 2D Cosserat-like micromorphic continua. We link this chirality to grain-scale mechanics using GMA. We then give an example of a granular system in which the desired grain-scale mechanism manifests at the macro-scale due to its micro-mechano-morphology. We show that macro-scale Cosserat chirality emerges in granular materials in which additional kinematical descriptors are required to accurately model the grain relative displacements. Further, we present results from parametric simulations to expound the effect of chirality on response at the macro-scale. These efforts are motivated from the view of designing experiments where such effects could be measured, and the necessity of highlighting the complex mechanics of materials with granular micro-structures.

2. Continuum model

We consider a Cosserat-like micromorphic continuum whose kinematic variables are the displacement field $u_i(X_j,\ t)$ and the skew-symmetric micro-structure rotation tensor $\psi(X_j,\ t)$ which herein reduces to a scalar quantity because a two-dimensional model is taken into account. Using these kinematic fields – defined over a bi-dimensional domain – we introduce deformation measures which are able to describe properly the behavior of the medium. The indices in the subscript take values of 1 and 2 corresponding to the two Cartesian coordinate axes, and the summation convention over repeated indices (in the subscript) is implied unless noted otherwise. In particular, we deal with the linearized strain tensor E_{ij} defined, as usual,

$$E_{ij} = u_{(i,j)} = \frac{1}{2}\left(u_{i,j} + u_{j,i}\right) \tag{1}$$

in terms of the components of the gradient of the displacement (the comma denotes a partial differentiation with respect to the material coordinates X_i specified by the following index), the micro-rotation ψ and the micro-rotation gradient $\psi_{,j}$. In order to complete the description of the considered material, we also introduce some coupling terms which allow us to make provision for some exchange of energy between the different deformation mechanisms. Specifically, we want to introduce the micro–macro coupling term related to the micro–macro relative rotation, i.e.

$$\gamma = \frac{1}{2}(u_{1,2} - u_{2,1}) - \psi \text{ or } \mathrm{e}_{ij}\gamma = u_{[i,j]} - \mathrm{e}_{ij}\psi \tag{2}$$

where the term $u_{[i,j]}$ is easily recognized as the antisymmetric part of the gradient of the displacement and, thus, represents the macro rotation, and e_{ij} is 2D Levi-Civita symbol. Furthermore, to consider the chiral effect, we also take into account a coupling between the relative micro–macro rotation γ and the two stretching deformations E_{11} and E_{22}.

According to the assumed hypotheses, the expression of the deformation energy is given as

$$W = t\int_B \left[\frac{1}{2}\lambda(E_{11}+E_{22})^2 + \mu\left(E_{11}^2 + E_{22}^2 + 2E_{12}^2\right) + \beta\gamma^2 + \alpha\left(\psi_{,1}^2 + \psi_{,2}^2\right) + \eta\gamma(E_{11}+E_{22})\right] dB \tag{3}$$

where t is the (out-of-plane) thickness of the body B. Eq. (3) represents a linear elastic material that is invariant to rotational transformation, however, does not satisfy the mirror invariance, and hence, possesses chirality. Such a material yields isotropic classical (Cauchy) elasticity and is said to belong to symmetry class [SO(2)] and can be termed as hemitropic (Spencer, 2004). In Eq. (3) the coefficients λ, μ, and α are material stiffnesses, while β and η are termed coupling coefficients since these connect the micro- and macro-scales. Of course, all of them should be chosen in order to have a positive definiteness of the energy density in Eq. (3), i.e.,

$$\alpha > 0,\ \ \mu > 0,\ \ \left(\lambda + \mu + \beta \pm \sqrt{(\lambda+\mu-\beta)^2 + 2\eta^2}\right) > 0 \tag{4}$$

The Principle of Virtual Work, neglecting inertia and non-contact volumic terms, states that

$$-\delta W + \delta W^{\text{ext}} = 0 \tag{5}$$

for every portion of the considered bi-dimensional body B and for every virtual displacement δu_i as well as virtual rotation $\delta\psi$. The external virtual work compatible with the deformation energy W is

$$\delta W^{\text{ext}} = t\int_{\partial_\tau B} \tau_i \delta u_i \mathrm{d}s + t\int_{\partial_\Psi B} \Psi\delta\psi \mathrm{d}s \tag{6}$$

which is defined on the boundary of the bi-dimensional body B. Therefore, the external actions are τ_i and Ψ, i.e., the force per unit line and the micro-couple, respectively.

3. Links to granular mechanics

The problem of synthesis of a microstructure, or more generally the micro-mechano-morphology, that, after homogenization, will produce an energy of the kind shown in Eq. (3) is rather interesting and somehow challenging. We believe that a chiral micro-mechano-structure of the kind shown in Misra et al. (2020), De Angelo et al. (2019) may give an example of such a synthesis. We will pursue such rigorous homogenization in a future work. Here we show that it is possible to link the postulated deformation energy in Eq. (3) to the micro-mechano-morphological properties of materials with granular textures. In our work, we consider granular materials to be those for which the deformation energy can be represented by the aggregation of the deformation energies of interacting grain-pairs. Indeed, by considering this linkage we will reveal the micro-mechanisms that lead to the emergent macro-scale behavior represented by our hypotheses. The granular micromechanics approach (GMA) proposed by Misra and coworkers (see for example (Nejadsadeghi and Misra, 2019; Misra and Poorsolhjouy, 2017; Poorsolhjouy and Misra, 2019) provides a practical pathway for developing this linkage. At the spatial scale appropriate for continuum description, in which the material point represents the collective behavior of numerous grains or behavior of grain collections forming an RVE, the individual grains and their motions are latent (concealed). It is notable though that it is the grain motions that determine the deformation behavior of the body, that is the mapping of a continuum material point from undeformed to deformed configuration in a macro body composed of such material. In GMA, the continuum description is achieved by (i) expressing grain-scale motions of a discrete model of granular system, in terms of continuum kinematic measures; (ii) identifying

the volume average of grain-pair interaction energies with the macro-scale deformation energy density; and finally (iii) applying variational approach for defining stress/force conjugates of the kinematic variables, determining constitutive relations, and the governing Euler-Lagrange equations (Nejadsadeghi and Misra, 2019; Misra and Poorsolhjouy, 2017; Poorsolhjouy and Misra, 2019; Misra and Poorsolhjouy, 2016). The GMA has parallels with Piola's concepts of continuum description of materials as an approximation of a molecular view (dell'Isola et al., 2015; dell'Isola et al., 2014; Eugster and dell'Isola, 2017; Giorgio et al., 2017). In this sense, GMA can be viewed as a heuristic homogenization scheme that proceeds by postulating deformation energies in terms of interrelated discrete and continuum kinematic descriptors. The resultant deformation energy density of a continuum material point and the granular volume it represents are the same in GMA. The RVE, in this case, is defined as a volume of a granular system whose mechanical response (deformation energy density) remains the same as the volume is moved within a specimen. This RVE size depends upon the micro-mechano-morphological properties of the considered granular system. The GMA is unlike the classical homogenization schemes in which Hill-Mandel type conditions are defined as a basis for determining RVE size. We briefly describe the seminal aspects of GMA and utilize it to find equivalent deformation energy, as that postulated, in terms of the grain-pair deformation energies.

3.1. Identification of grain motions with continuum kinematic variables

Consider a 2D granular solid body which appears as a homogeneous continuum placed in a macro-scale Cartesian coordinate system denoted by X_i. The continuum material points of this solid body are formed of collection of grains. Further consider a micro-scale Cartesian coordinate system denoted by X_i', in which the grain locations and motions can be distinguished. Now attach the micro-scale coordinate system to the continuum material point, with its origin at the barycenter of the corresponding volume element and its coordinate axes parallel to the macro-scale coordinate system X_i as shown in Fig. 1. Utilizing the two coordinate systems, the displacement field of grain centroids, ϕ_i, under an arbitrary deformation of this granular solid can be written as (Nejadsadeghi and Misra, 2019)

$$\phi_i = u_i(X_m) + \psi_{ij}^{\phi}(X_m)X_j' + \psi_{ijk}^{\phi}(X_m)X_j'X_k' \tag{7}$$

considering by choice the displacement fields to be up to 2nd order in terms of micro-scale coordinates, although higher-order terms can be considered as discussed in [24]. In Eq. (7);u_i is the macro-scale displacement field, and quantities ψ_{ij}^{ϕ} and ψ_{ijk}^{ϕ}, functions of macro-scale coordinates X_m, are termed as the second and the third rank micro-deformation tensors. The assumption in Eq. (7) permits description of fluctuations in grain displacement with respect to the macro-scale displacement field. These fluctuations have been observed in experiments on grain packings and have been widely commented in literature on granular and other disordered systems as non-affine grain motions [36–41]. The non-affinity arises due to a variety of factors, including irregularity of granular structure, spatial variability and high contrast of grain interactions (stiff or soft), and the peculiar and non-local nature of grain interactions. Using Eq. (7), the displacement of the grain p centroid can be written in terms of the displacement of the neighbor interacting grain, n, centroid as follows

$$\delta_i^{np} = \phi_i^p - \phi_i^n = \psi_{ij}^{\phi} l_j^{np} + \psi_{ijk}^{\phi} J_{jk}^{np} \tag{8}$$

where $l_j^{np} = X_j'^p - X_j'^n$ is a grain-pair branch vector joining the centroids of grains n and p, the tensor product $J_{jk}^{np} \approx l_j^{np} l_k^{np}/2$ is the gyration tensor. To understand the geometrical nature of the micro-deformation tensors, it is useful to consider the following relative deformation tensors

$$\gamma_{ij}^{\phi} = u_{i,j} - \psi_{ij}^{\phi} \text{ and } \gamma_{ijk}^{\phi} = \psi_{ij,k}^{\phi} - \psi_{ijk}^{\phi} \tag{9}$$

where comma in the subscript denotes differentiation with respect to the macro-scale coordinates X_i, and defines the macro-scale gradients of the macro displacement field u_i, and micro-deformation tensor ψ_{ij}^{ϕ}.

In view of the hypotheses in Eq. (3) and the kinematic variables of the continuum model in Eqs. (1) and (2), Eq. (9) is simplified by assuming that only the skew-symmetric part of the relative deformation is non-vanishing given by the relative rotation in Eq. (2) such that $\psi_{(ij)}^{\phi} = u_{(i,j)} = E_{ij}$. Further, we assume that the 3rd rank relative deformation tensor γ_{ijk}^{ϕ} vanishes such that the 3rd rank micro-deformation tensor, ψ_{ijk}^{ϕ}, is no longer and independent measure but it is related to the macro-scale gradient of the 2nd rank micro-

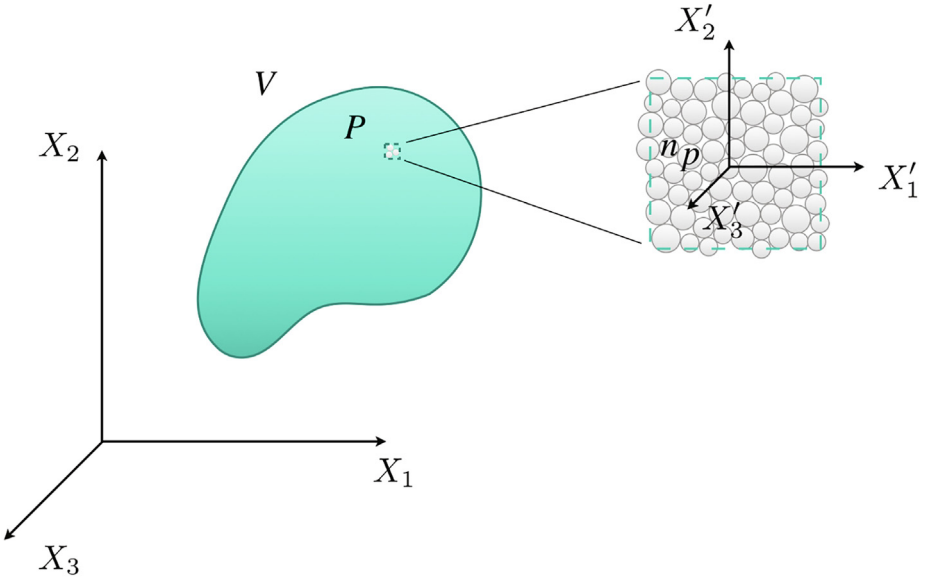

Fig. 1. Schematic of the continuum material point, P, and its granular microstructure magnified for visualization, where the x' coordinate system is attached to its barycenter.

deformation tensor, $\psi^{\phi}_{ij,k}$. The assumption is analogous to the simplification of kinematic measures to go from a Timoshenko beam model to an Euler beam model by relating the rotational degree of freedom to the gradient of deflection. Moreover, we retain only the gradients of skew-symmetric part of micro-deformation tensor, $\psi^{\phi}_{[ij]}$, such that $\psi^{\phi}_{ijk} = \psi^{\phi}_{[ij],k} = e_{ij}\psi_{,k}$ and the kinematic descriptors of the resulting model are the same as that in the assumed continuum model.

In this case, the displacement of a grain centroid given in Eq. (7), and consequently, the relative displacement of two neighbor grains, n and p, in Eq. (8) will simplify to (using the kinematic variables defined in Eqs. (1) and (2))

$$\delta^{np}_i = \phi^p_i - \phi^n_i = E_{ij}l^{np}_j - e_{ij}\gamma l^{np}_j + e_{ij}\psi_{,k}J^{np}_{jk} = \delta^M_i - \delta^m_i + \delta^g_i \tag{10}$$

where we ensure that the macro-rotations do not result in relative movements. Clearly, the relative displacement between grains (n and p in our case) can be decomposed into components related to the macro-strain, E_{ij}, the micro–macro relative rotation, γ, and the macro-gradient of the micro-rotation field ψ, are, respectively, such that for a generic grain-pair denoted by a (representing interacting grains such as n and p)

$$\delta^{aM}_i = E_{ij}l^a_j;\ \delta^{am}_i = e_{ij}\gamma l^a_j;\ \delta^{ag}_i = e_{ij}\psi_{,k}J^a_{jk} \tag{11}$$

Thus, Eqs. (10) and (11) provide an identification of the continuum kinematic variables with those of the grain motion. It is noteworthy that the micro–macro relative rotation in Eq. (2) and the micro-rotation field ψ, do not consider grain spins. The micro-rotation appears to be simply a manifestation of non-symmetric gradients of displacement at the micro-scale and do not imply grain rotation or spin. Indeed grain spin or rotation could be significant in some granular systems [30] and are known from measurements of kinematic fields in grain assemblies [36,37] as well as simulation using discrete granular models [42,43]. For further discussions of GMA based higher-order models, the reader is directed to [24] which describes in details the kinematics of micromorphic model of degree n as well as its devolution to micromorphic models of degrees 2 and 1, and to micro-polar models and 2nd gradient models.

3.2. Deformation energy equivalence and 2D constitutive relationship

Using the grain-scale and continuum kinematic identification, the deformation energy density, $\bar{W}$, in Eq. (3) can be expressed in terms of grain-scale kinematic measures as follows:

$$\bar{W} = \bar{W}\left(E_{ij}, \gamma, \psi_{,k}\right) = \frac{1}{V}\sum\nolimits_a W^a\left(\delta^{aM}_i, \delta^{am}_i, \delta^{ag}_i\right) \tag{12}$$

where W^a is the grain-pair deformation energy and the summation is over all grain-pairs, denoted by a, within the volume element forming the continuum material point.

The grain-pair deformation can be considered in a local Cartesian coordinate system formed of the unit vector along the axis joining the centroids of the two grains, termed as the normal direction, and unit vector orthogonal to the normal direction, termed as the tangential plane. For the case of 2D granular systems, the grain-pair interactions are defined in the local coordinate system composed of a unit normal vector, n_i, along the line that connects the grain centroids, and the tangential unit vector, s_i, orthogonal to n_i, given as

$$\begin{aligned} n_i &= \langle n_1, n_2\rangle = \langle \cos\theta, \sin\theta\rangle \\ s_i &= \langle s_1, s_2\rangle = \langle -\sin\theta, \cos\theta\rangle \end{aligned} \tag{13}$$

where θ is the polar angle of the 2D polar coordinate system. The grain-pair elastic deformation energy can now be defined in terms of the grain-scale kinematic quantities and stiffnesses, based upon a particular constitutive choice, as follows

$$W^a = \frac{1}{2}\left[K^{aM}_n\left(\delta^{aM}_n\right)^2 + K^{aM}_s\left(\delta^{aM}_s\right)^2 + K^{am}_s\left(\delta^{am}_s\right)^2 + 2K^{am}_{ns}\left(\delta^{aM}_n\delta^{am}_s\right) + K^{ag}_s\left(\delta^{ag}_s\right)^2\right] \tag{14}$$

In Eq. (14) the subscripts are used to denote the quantities along the local coordinate axes (these subscripts do not follow tensor summation convention), such that

$$\delta^{aM}_n = E_{ij}l^a_j n^a_i;\ \delta^{aM}_s = E_{ij}l^a_j s^a_i;\ \delta^{am}_s = e_{ij}\gamma l^a_j s^a_i;\ \delta^{ag}_s = e_{ij}\psi_{,k}J^a_{jk}s^a_i \tag{15}$$

and it can be shown that components of δ^{am}_i and δ^{ag}_i along vector, n_i, vanish, that is $\delta^{am}_n = e_{ij}\gamma l^a_j n^a_i = 0$; $\delta^{ag}_n = e_{ij}\psi_{,k}J^a_{jk}n^a_i = 0$. We also note that in Eq. (14) the coupling terms have been retained only for the grain-pair relative displacement components related to the micro–macro relative rotations and macro-strain. This constitutive choice of deformation energy in Eq. (14) will lead to the desired particular form of continuum model given in Eq. (3).

The constitutive relationships can now be established recognizing that macro-scale stress measures can be defined as conjugates

Table 1
Micro-scale stiffnesses (kN/mm).

K^M_n	K^M_s	K^m_s	K^m_{ns}	K^g_s
8.4	4.2	3.0	2.07	0.1×10^7

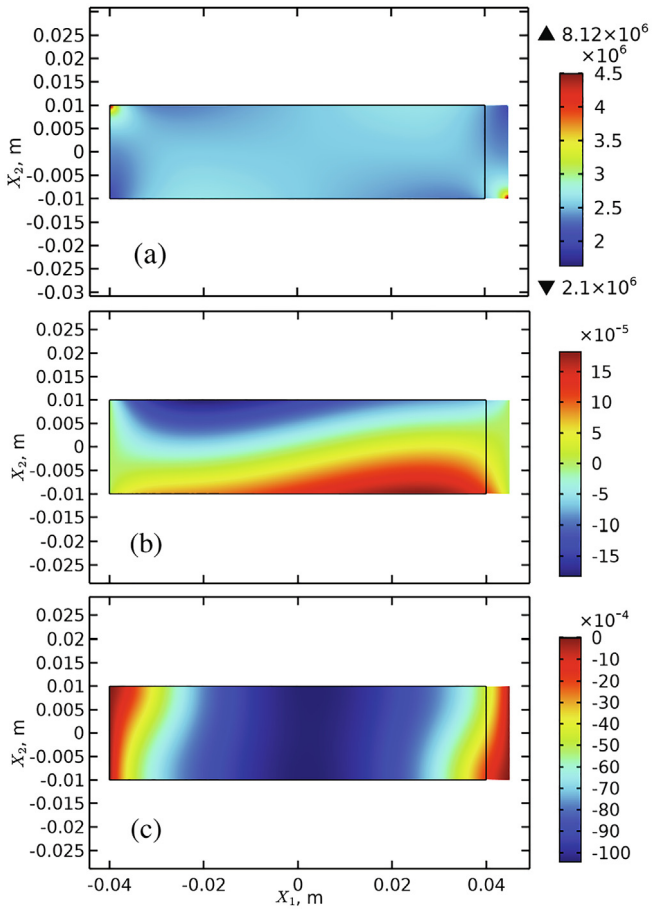

Fig. 2. Extension test with zero boundary conditions on ψ: stored energy density a); displacement u_2 b); micro-rotation ψ c).

to each of the continuum kinematic variables, (see for example [25])

$$\tau_{ij} = \frac{\partial \bar{W}}{\partial E_{ij}} = C^M_{ijkl}E_{kl} + \eta\delta_{ij}\gamma;$$
$$\sigma = \frac{\partial \bar{W}}{\partial \gamma} = 2\beta\gamma + \eta(E_{11}+E_{22});\ \mu_k = \frac{\partial \bar{W}}{\partial \psi_{,k}} = 2\alpha\psi_{,k} \tag{16}$$

In Eq. (16),τ_{ij}, is the symmetric Cauchy stress, and σ is the relative moment stress, μ_k is the double moment stress, and C^M_{ijkl} is the standard isotropic elastic tensor formed by the standard Lame's coefficients λ and μ (Eq. (3)). The passage from the summation in Eq. (12) to integration through a directional averaging process for isotropic aggregates of granular structures and the identification of the constitutive coefficient in Eqs. (3) and (14) for given granular structures have been described in [25,44]. Consequently, it is possible to link the grain-scale stiffness parameters with the macro coefficients of Eq. (3) as given below.

$$\lambda = \frac{l^2\rho^c}{8}\left(K^M_n - K^M_s\right);\ \mu = \frac{l^2\rho^c}{16}\left(K^M_n + K^M_s\right);$$
$$\beta = 4\frac{l^2\rho^c}{8}\left(K^m_s\right);\ \alpha = \frac{l^4\rho^c}{8}\left(K^g_s\right);\ \eta = 2\frac{l^2\rho^c}{8}\left(K^m_{ns}\right) \tag{17}$$

In Eq. (17), the grain-scale stiffness parameters and grain-size l, represent average values as defined in the Appendix and in [26], and ρ^c is the number density of grain-pair interactions. We further note that the coupling between the relative micro–macro rotation γ and the two stretching deformations E_{11} and E_{22}, is widely overlooked in the literature on Cosserat and micro-polar solids (see for example [10]), although this type of chiral coupling has been utilized recently for describing certain lattice structures [12,13]. The analysis presented shows that for a granular material to exhibit chiral Cosserat effects of the type postulated in Eq. (3), the description of grain-scale kinematics (1) must include the quantities, γ and ψ, as given in Eq. (10), and (2) the grain-pair relative displacement caused by these quantities must store energy. Consequently,

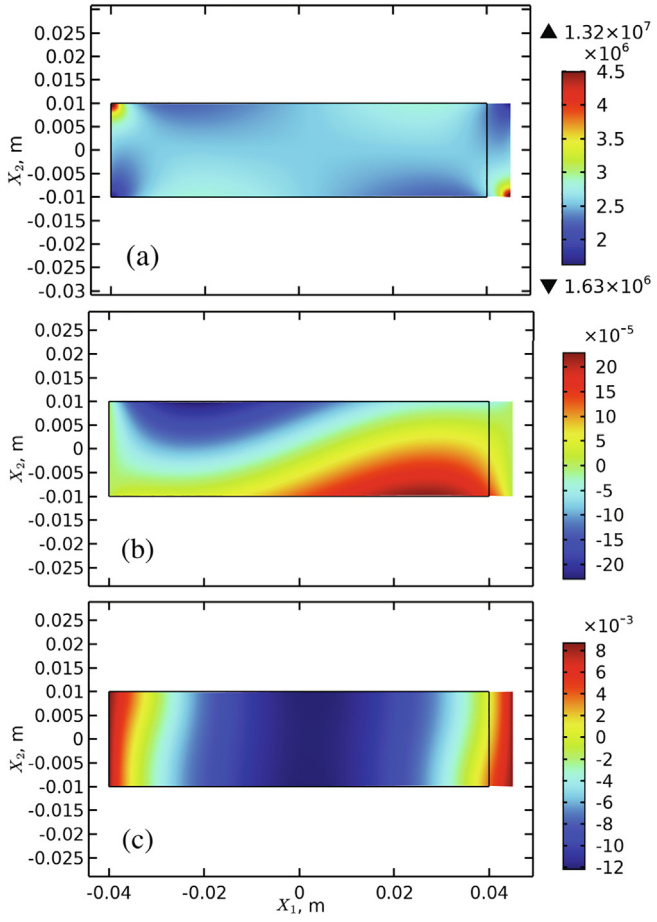

Fig. 3. Extension test with an imposed value of ψ equal to $\pi/360$: stored energy density a) displacement u_2 b) micro-rotation ψ c).

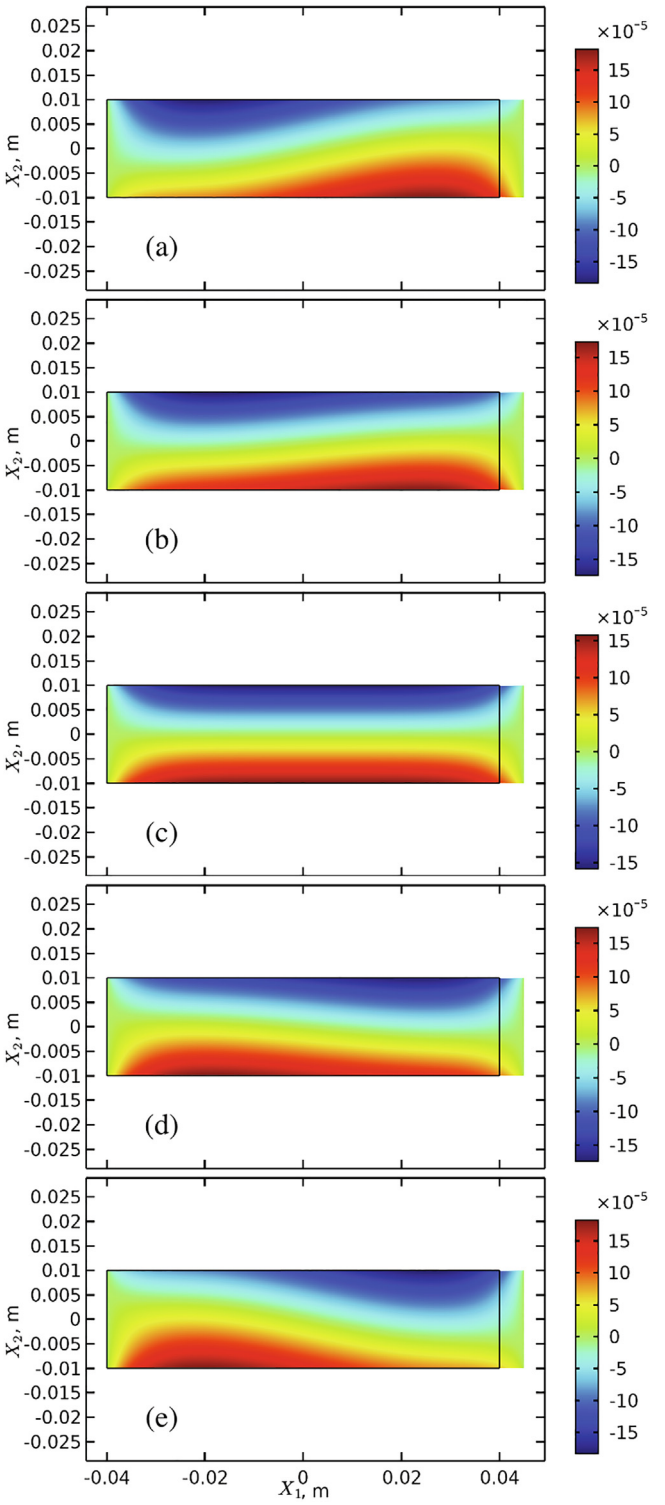

Fig. 4. Displacement u_2 in an extension test with zero boundary conditions on ψ: $K^m_{ns} = 2.07$a); $K^m_{ns} = 1.035$b); $K^m_{ns} = 0$c); $K^m_{ns} = -1.035$d); $K^m_{ns} = -2.07$e). Non-uniform Poisson's effect along the x-axis, and non-invariance to reflection about x-axis is observed for non-zero coupling parameter K^m_{ns}.

the synthesis of a granular micro-structure, or more generally micro-mechano-morphology, must satisfy these requirements. Such effects are indeed present in granular microstructures as seen from the identification given in [44], and the micro-mechano effects have been further expounded recently through analyses and experiments on 1D structures modeled as granular materials [26,27].

4. Results and discussions

To examine the effect of chirality we have performed numerical simulations of simple extension and simple shear with the proposed bi-dimensional continuum model. In particular, these simulations intend to illustrate measureable effects that chirality induces at the boundaries and the bulk body under loading conditions that can be physically realized in laboratories. The numerical simulations have been performed using the commercial software COMSOL Multiphysics, which allows us to solve the Eq. (5) directly resorting to a standard finite element formulation. Further to illustrate the link between the postulated continuum model and granular material that exhibit significant chirality we consider a case study for which the values of micro-stiffness are those listed in Table 1. These micro-stiffness are guided by the identification presented for regular granular structures presented by the corresponding author in [44], particularly for structure designated as assembly C. In these calculations we also assume that the average grain size l = 22 μm and $\rho^c = 1384$ mm^{-3} for a representative volume element of size 1 mm^3. We note that in order to highlight the nature of chiral behavior, we have modified micro-stiffness, K_s^g (from that in [44]). The modification is to enhance the thickness of the boundary layer such that the effect of chirality can be easily visualized, although such effects are present in weakly chiral med-

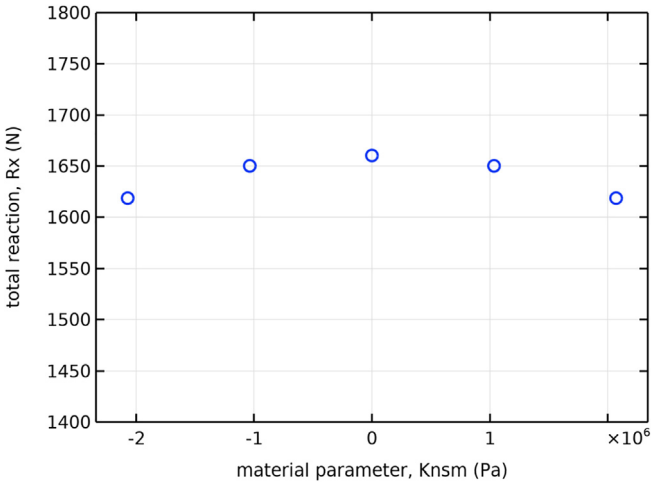

Fig. 6. Resultant reaction in the x-direction, showing a reduction for non-zero coupling stiffness K_{ns}^m.

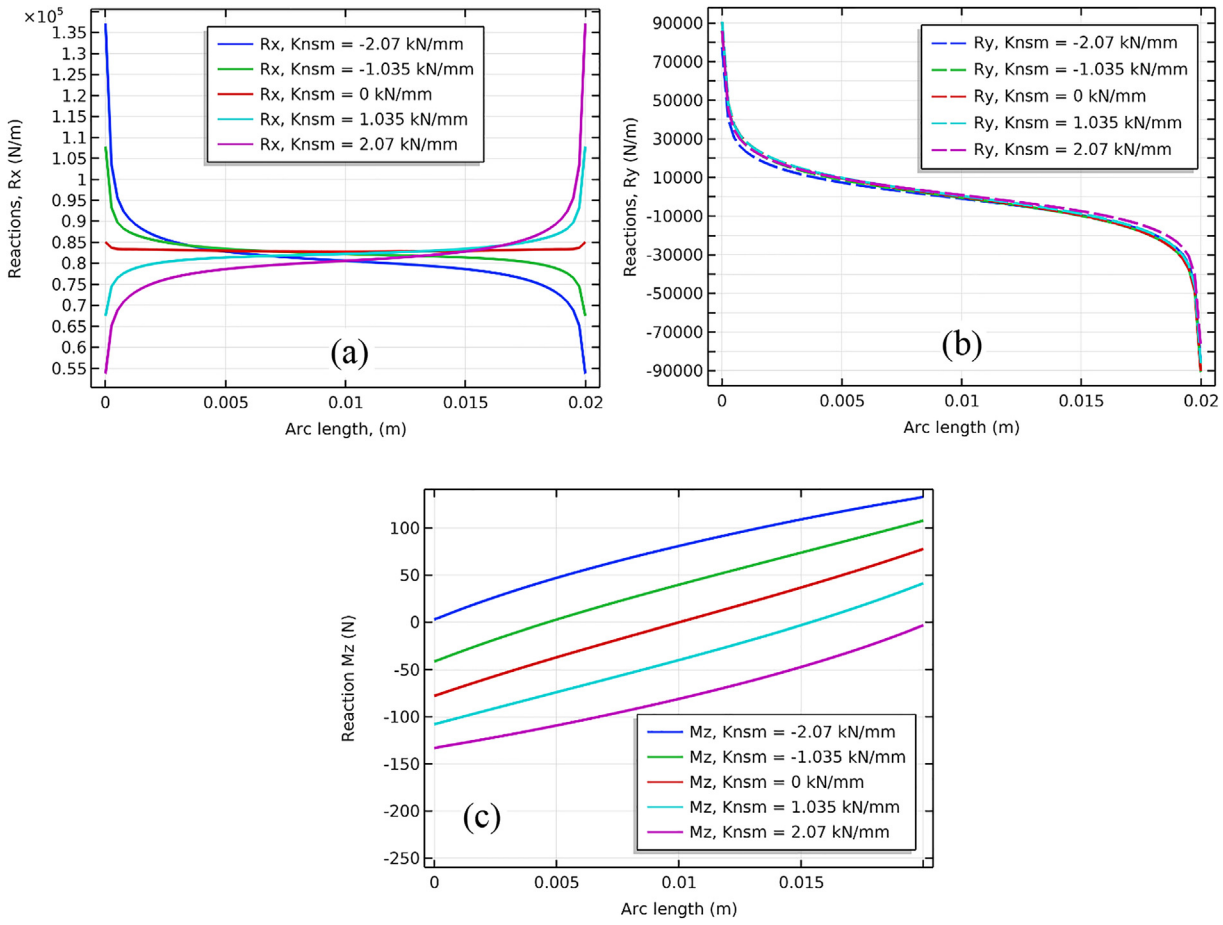

Fig. 5. Distribution of reactions (along x- and y- directions and moments) along the right boundary for the five cases simulated in Fig. 5. (a) The reaction is distributed non-symmetrically in the x-direction and does not satisfy reflection invariance about the x-axis for non-zero coupling parameter K_{ns}^m. (b) The reaction in the y-direction is distributed anti-symmetrically so as to yield a vanishing resultant. (c) Moments also show non-symmetric distribution. For zero coupling parameterK_{ns}^m, the moment is anti-symmetrically distributed yielding vanishing resultant, for all other cases, a non-zero moment resultant is obtained.

ium and in solids with weak Cosserat effect and could be significant in determining its mechanical response.

4.1. Simple extension

Using the reported parameters, a simple extension test was simulated for a rectangular planar body (20 × 80 mm dimension) locking the left short edge and imposing a given longitudinal displacement at the right short edge, while the micro rotation ψ are kept null on these two edges, as follows:

$$u_1(0,X_2) = u_2(0,X_2) = u_2(L,X_2) = 0;\ u_1(L,X_2) = 5mm;\\ \psi(0,X_2) = \psi(L,X_2) = 0; \tag{18}$$

The Fig. 2 shows the chiral effect, which is clear for the lack of symmetry evident in the total stored energy density as well as in the transversal displacement u_2. A clear measurable outcome is the lack of uniformity (in addition to the asymmetry) of Poisson's effect as seen from the distribution of transversal displacement u_2. In addition, it may also be possible to measure micro-rotations in the center region of the body as seen from the distribution of micro-rotation ψ. Fig. 3 displays the effect of the boundary condition on micro-rotation ψ. Indeed, imposing a very small value, different from zero, to ψ, we can observe a more noticeable chiral effect both in the energy density and in the displacement (in this case the boundary condition for displacement is given in Eq. (18), while for micro-rotation is: $\psi(0,X_2) = \pi/360$;

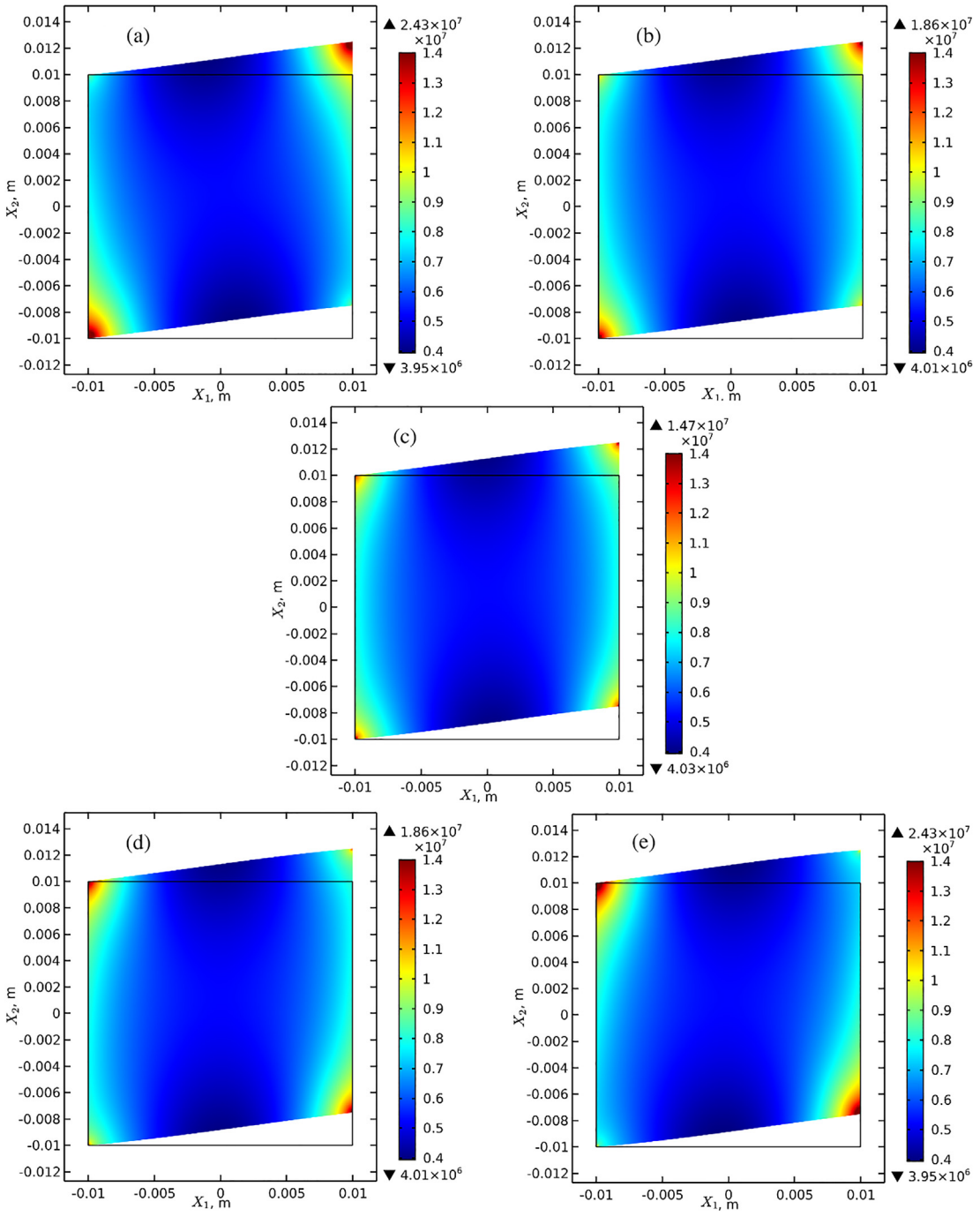

Fig. 7. Deformation energy density in a shear test with zero boundary conditions on ψ: $K^m_{ns} = 2.07$a); $K^m_{ns} = 1.035$b); $K^m_{ns} = 0$c); $K^m_{ns} = -1.035$d); $K^m_{ns} = -2.07$e). The deformation energy density related to the chiral coupling is symmetric for zero coupling parameter K^m_{ns}, while it is asymmetric for non-zero coupling parameter K^m_{ns}.

$\psi(L, X_2) = \pi/360$). Finally, we investigate the influence of the chiral coupling term performing a parametric analysis on the coefficient η, that is changing the micro-mechano structural coupling parameter K_{ns}^m. This parametric study is performed for the boundary condition in Eq. (18). The results are summarized in Fig. 4 where it is clear that the chiral effect corresponds in amount to the value of the considered parameter and when it is zero no chiral effect is present. Both the asymmetric distribution of the transversal displacement u_2, and non-uniformity of Poisson's effect show marked severity with increasing value of the coupling parameter.

Further emphasizing the viewpoint of measureable effects, we present in Fig. 5, the x- and y-components of reaction forces and reaction moments (micro-couple) along the edge with specified displacement and micro rotation, for the five cases simulated in Fig. 5. As defined in Eq. (6), the reactions forces and moments are the conjugates of the specified displacement and micro rotation. From a numerical viewpoint, the constrained reactions Rx, Ry, and Mz have directly been evaluated as Lagrange multipliers associated with the essential boundary conditions (18) and (19). We observe that the x-component of reaction force has a non-symmetrical distribution along the edge when the coupling parameter K_{ns}^m is non-zero. In fact, the force concentration at the two corners show a significant difference. It is notable however that the resultant y-component of reaction force vanishes since it is distributed anti-symmetrically along the edge given the clamped boundary conditions. The reaction moments also have a non-symmetric distribution. For zero coupling parameter K_{ns}^m, the moment is anti-symmetrically distributed yielding vanishing resultant. For all other cases, a non-zero moment resultant is obtained. Finally, we observe in Fig. 6 that the resultant x-component of reaction force decreases with increasing numerical (absolute) value of coupling parameter K_{ns}^m increases.

4.2. Simple shear

Simple shear test was also simulated for a square planar body (20×20 mm dimension) locking left edge and imposing a given transversal displacement at the right edge, while the micro rotation ψ are kept null on these two edges, as follows:

$$\begin{aligned} u_1(0, X_2) = u_1(L, X_2) = 0; \\ u_2(0, X_2) = 0;\ u_2(L, X_2) = 2.5mm; \\ \psi(0, X_2) = \psi(L, X_2) = 0; \end{aligned} \tag{19}$$

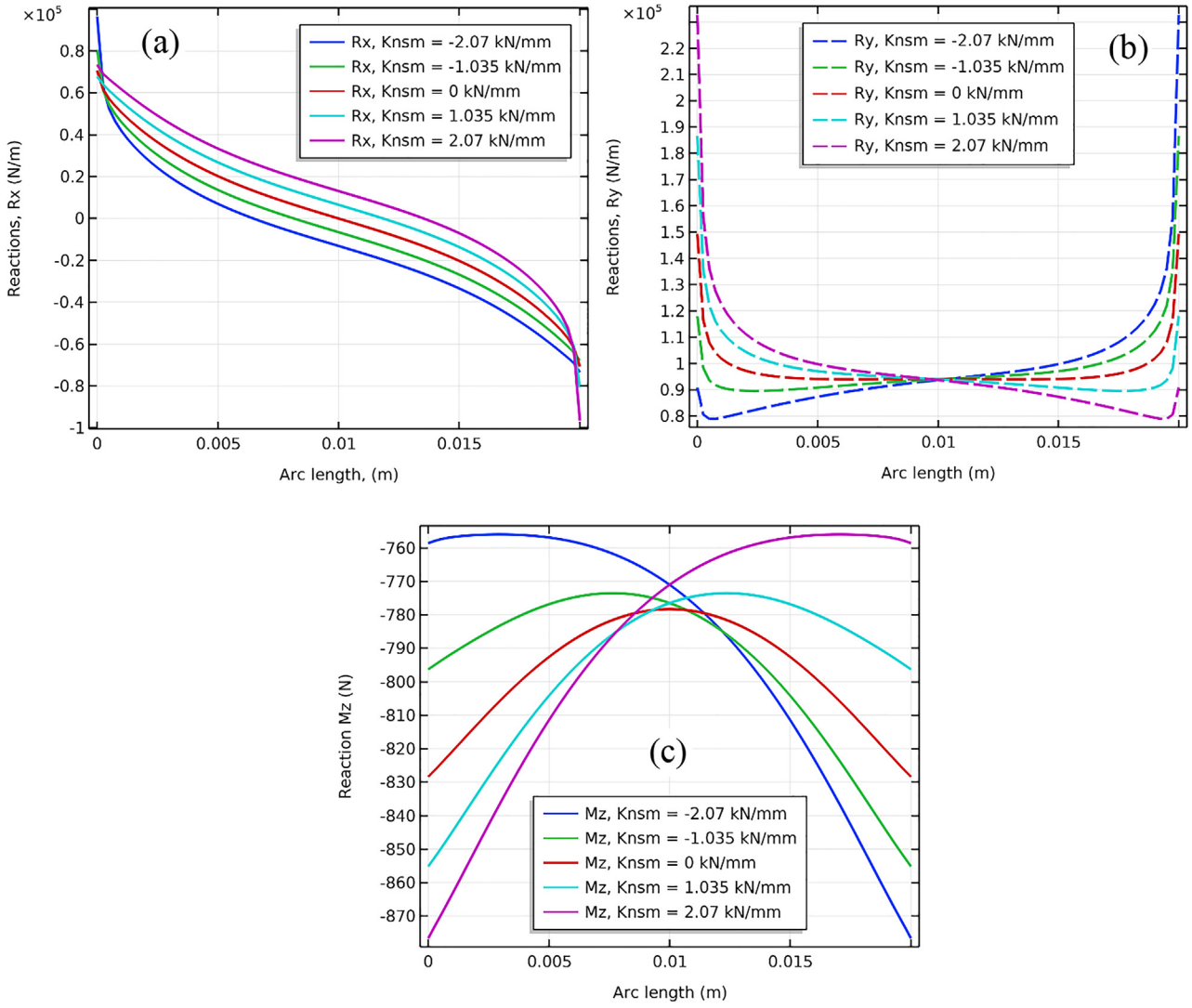

Fig. 8. Distribution of reactions (along x- and y- directions and moments) along the right boundary for the five shear tests simulated in Fig. 8. (a) The reaction in the x-direction is distributed anti-symmetrically so as to yield a vanishing resultant. (b) The reaction is distributed non-symmetrically in the y-direction and does not satisfy reflection invariance about the x-axis for non-zero coupling parameter K_{ns}^m. (c) Moments also show non-symmetric distribution except for zero coupling parameter K_{ns}^m, for which the moment is symmetrically distributed.

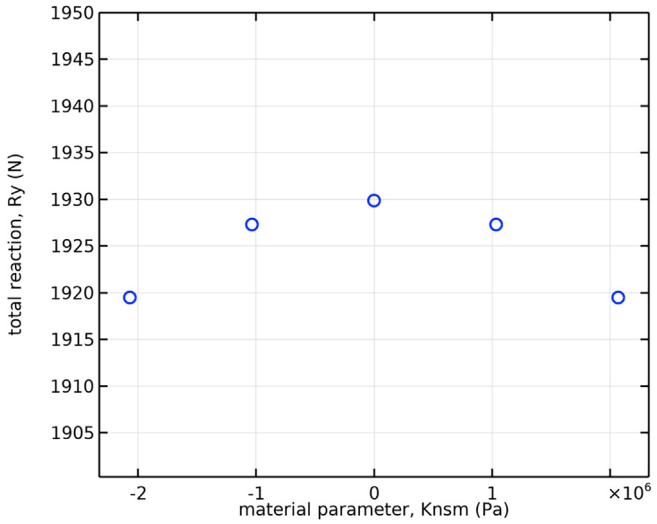

Fig. 9. Resultant reaction in the y-direction, showing a reduction for non-zero coupling stiffness K_{ns}^{m}.

The Fig. 7 shows the effect of chirality in the total stored energy density. For the case of zero coupling parameter K_{ns}^{m}, the deformation energy density is symmetric with respect to the concentrations at the corners (Fig. 7c). It is notable here that for classical Cauchy continua, the deformation energy under simple shear will be uniform. The boundary layers and concentrations at the corners that develop are the consequence of micro-rotation degree-of-freedom (Cosserat effect). Further, the chiral coupling term results in an asymmetric distribution of deformation energy density concentrate reducing and emphasizing the energy concentrations at opposite corners. The sign of the coupling parameter, K_{ns}^{m}, determines the maximal and minimal corners.

Again, from the viewpoint of measureable effects, we present in Fig. 8, the x- and y-components of reaction forces and reaction moments along the edge with specified displacement and micro rotation, for the five cases simulated in Fig. 7. We observe that the y-component of reaction force has a non-symmetrical distribution along the edge when the coupling parameter K_{ns}^{m} is non-zero. In fact, the force concentration at the two corners show a significant difference. It is notable however that the resultant x-component of reaction force vanishes since it is distributed anti-symmetrically along the edge. The vanishing x-component resultant is not unexpected in a simple shear deformation. Finally, we note that reaction moments have a non-symmetric distribution except for the case of zero coupling parameter K_{ns}^{m}. In all the cases though, we obtain a non-zero moment resultant. Finally, we observe in Fig. 9 that the resultant y-component of reaction force decreases with increasing numerical (absolute) value of coupling parameter K_{ns}^{m}

5. Summary and conclusion

We have presented a Cosserat-like micromorphic continuum model and its links to micro-scale mechanism in granular materials. The presented effort is a step towards addressing the general problem of finding a microstructure, which, upon homogenization, results in the postulated macro-scale deformation energy, such as that in Eq. (3). In this work, we consider the equivalence of postulated deformation energy in the continuum model with that of the granular model in which the granular micromechanics approach (GMA) is used for the identification of grain-scale motion with continuum kinematic variables. The continuum parameter that leads to chiral behavior is then identified with that at the grain-scale. We have shown that the micro-rotation is simply a manifestation of non-symmetric gradients of displacement at the micro-scale and do not imply grain rotation or spin, and the energy stored in micro-rotation is related to the coupling between the normal and shear response of grain-pairs.

Example of a granular material in which the desired grain-scale behavior can be obtained is presented. Parametric simulations are also presented to expound the effect of chirality on response at the macro-scale. Furthermore, from the viewpoint of measureable effects, reaction forces and moments at the boundary are calculated under simple extension and simple shear test. Interesting asymmetries in force concentrations and non-zero boundary moments emerge as a characteristic of these materials. Future studies will aim to identify the grain-scale mechanisms that can tie the continuum models more strongly to the micro-scale mechanics and develop rigorous homogenization schemes.

Declaration of Competing Interest

The authors declare that they have no known competing financial interests or personal relationships that could have appeared to influence the work reported in this paper.

Acknowledgement

This research is supported in part by the United States National Science Foundation grant CMMI -1727433.

Appendix

As an example, we evaluate the second of Eq. (16), written here in expanded form as using Eqs. (14) and (15)

$$\begin{aligned}\sigma &= \frac{\partial \bar{W}}{\partial \gamma} = \frac{1}{V}\sum_a \frac{\partial W^a}{\partial \gamma} = \frac{1}{V}\sum_a \frac{\partial W^a}{\partial \delta_s^{am}}\frac{\partial \delta_s^{am}}{\partial \gamma} = \frac{1}{V}\sum_a \left(K_s^{am}\delta_s^{am} + K_{ns}^{am}\delta_n^{aM}\right)\frac{\partial \delta_s^{am}}{\partial \gamma} \\ &= \frac{1}{V}\left(\sum_a K_s^{am} e_{ij} l_j^a s_i^a e_{pq} l_q^a s_p^a\right)\gamma + \frac{1}{V}\left(\sum_a K_{ns}^{am} e_{ij} l_j^a s_i^a l_q^a s_p^a E_{pq}\right)\end{aligned} \tag{20}$$

Thus, we get the following

$$\beta = \frac{1}{2V}\sum_a K_s^{am} e_{ij} l_j^a s_i^a e_{pq} l_q^a s_p^a;\ \ \eta(E_{11}+E_{22}) = \frac{1}{V}\sum_a K_{ns}^{am} e_{ij} l_j^a s_i^a l_q^a s_p^a E_{pq} \tag{21}$$

Since the summation in Eq. (21) is over all the grain-pair, it can be sorted and binned according to grain-pair orientations and recast as summation over the polar angle θ as

$$\begin{aligned}\beta &= \frac{1}{2V}\sum_\theta \left(\sum_\rho^{N^\rho} \left(l^\rho\right)^2 K_s^{\rho m}\right) e_{ij} n_j^\theta s_i^\theta e_{pq} n_q^\theta s_p^\theta; \\ \eta(E_{11}+E_{22}) &= \frac{1}{V}\sum_\theta \left(\sum_\rho^{N^\rho} \left(l^\rho\right)^2 K_{ns}^{\rho m}\right) e_{ij} n_j^\theta s_i^\theta \left(n_q^\theta s_p^\theta E_{pq}\right)\end{aligned} \tag{22}$$

where $N^\rho(\theta)$ is the total number of grain-pair for a given polar angle bin θ, such that

$$N = \sum_\theta N^\rho(\theta) \tag{23}$$

where N is the count of grain-pairs in the RVE and the summation over ρ is the sum of the product of branch length square and the grain-pair stiffness (for example $\left(l^\rho\right)^2 K_{ns}^{\rho m}$) for all grain-pairs in that bin. For granular material systems with many different grain-sizes, grain shapes and types of grain-pair interactions (which as combination can be termed as micro-scale mechano-morphology), these sums will be different for different polar angles. This variation with polar angles can be treated by defining directional distribution

functions. Since branch length and stiffnesses appear as products, their directional distribution density cannot be defined independently, therefore, we introduce the directional density distribution function, $\xi(\theta)$, defined as

$$\xi(\theta) = \frac{\sum_{\rho} \left(l^{\rho}\right)^2 K_s^{\rho m}}{\sum_{a=1}^{N} \left(l^{a}\right)^2 K_s^{am}} = \frac{\sum_{\rho} \left(l^{\rho}\right)^2 K_{ns}^{\rho m}}{\sum_{\alpha=1}^{N} \left(l^{a}\right)^2 K_{ns}^{am}} \tag{24}$$

where, for simplicity, we have assumed that grain-pair behavior follow the same distribution. For materials with direction independence, the density distribution function in 2D domains is simply

$$\xi(\theta) = \frac{1}{2\pi} \Rightarrow \int_{\theta} \xi d\theta = \frac{1}{2\pi} 2\pi = 1; \tag{25}$$

It is evident that the directional density distribution function, $\xi(\theta)$, represents the relative measure of material stiffness in a given direction resulting from a combination of grain-size, the number of grain-pair interactions and the grain-pair stiffness. Further, it is useful to define an average product of branch length square and the grain-pair stiffness, $l^2 K_n$, as

$$l^2 K_s^m = \frac{\sum_{a=1}^{N} \left(l^{a}\right)^2 K_s^{am}}{N}; \quad l^2 K_{ns}^m = \frac{\sum_{a=1}^{N} \left(l^{a}\right)^2 K_{ns}^{am}}{N} \tag{26}$$

where l may be regarded as the average branch length, K_n^M and K_s^M as the average grain-pair stiffnesses for the material, and $\rho^c = V/N$ is the number density of grain-pair interactions. Thus, using Eqs. (13), 24 and 26, the following integral form of Eq. (22) can be obtained

$$\begin{aligned} \beta &= l^2 \rho^c \int_{\theta=0}^{\pi} \left(K_s^m e_{ij} n_j s_i e_{pq} n_q s_p\right) \xi d\theta = l^2 \rho^c \int_{\theta=0}^{\pi} K_s^m \xi d\theta \\ \eta(E_{11} + E_{22}) &= l^2 \rho^c \int_{\theta=0}^{\pi} \left(K_{ns}^m e_{ij} n_j s_i n_q s_p E_{pq}\right) \xi d\theta \\ &= l^2 \rho^c \int_{\theta=0}^{\pi} -K_{ns}^m \left(E_{11}\cos^2\theta + E_{22}\sin^2\theta + E_{12}\sin 2\theta\right) \xi d\theta \end{aligned} \tag{27}$$

which using density distribution function, $\xi(\theta)$, for directionally independent system in Eq. (25), yields the expression for β and η in Eq. (17). The other elastic constants are obtained in a similar manner.

References

Abdoul-Anziz, H., Seppecher, P., 2018. Strain gradient and generalized continua obtained by homogenizing frame lattices. Math. Mech. Complex Systems 6 (3), 213–250.

Alibert, J.-J., Seppecher, P., Dell'Isola, F., 2003. Truss modular beams with deformation energy depending on higher displacement gradients. Math. Mech. Solids 8 (1), 51–73.

Altenbach, J., Altenbach, H., Eremeyev, V.A., 2010. On generalized Cosserat-type theories of plates and shells: A short review and bibliography. Arch. Appl. Mech. 80 (1), 73–92.

Andreaus, U., Spagnuolo, M., Lekszycki, T., Eugster, S.R., 2018. A Ritz approach for the static analysis of planar pantographic structures modeled with nonlinear Euler-Bernoulli beams. Continuum Mech. Thermodyn. 30 (5), 1103–1123.

Auffray, N., Dirrenberger, J., Rosi, G., 2015. A complete description of bi-dimensional anisotropic strain-gradient elasticity. Int. J. Solids Struct. 69, 195–206.

Barchiesi, E., Ganzosch, G., Liebold, C., Placidi, L., Grygoruk, R., Müller, W.H., 2019. Out-of-plane buckling of pantographic fabrics in displacement-controlled shear tests: Experimental results and model validation. Continuum Mech. Thermodyn. 31 (1), 33–45.

Barchiesi, E., Placidi, L., 2017. A review on models for the 3D statics and 2D dynamics of pantographic fabrics, in Wave dynamics and composite mechanics for microstructured materials and metamaterials. Springer, pp. 239–258.

Berkache, K., Deogekar, S., Goda, I., Picu, R.C., Ganghoffer, J.-F., 2019. Identification of equivalent couple-stress continuum models for planar random fibrous media. Continuum Mech. Thermodyn. 31 (4), 1035–1050.

Chen, Y., Liu, X., Hu, G., Sun, Q., Zheng, Q., 2014. Micropolar continuum modelling of bi-dimensional tetrachiral lattices. Proc. Royal Soc. A: Math. Phys. Eng. Sci. 470 (2165), 20130734.

Cosserat, E., Cosserat, F., 1909. Theory of Deformable Bodies. Scientific Library A. Hermann and Sons, Paris.

De Angelo, M., Placidi, L., Nejadsadeghi, N., Misra, A., 2019. Non-standard Timoshenko beam model for chiral metamaterial: Identification of stiffness parameters. Mech. Res. Commun. 103462

dell'Isola, F., Andreaus, U., Placidi, L., 2015. At the origins and in the vanguard of peridynamics, non-local and higher-gradient continuum mechanics: An underestimated and still topical contribution of Gabrio Piola. Math. Mech. Solids 20 (8), 887–928.

dell'Isola, F., Giorgio, I., Pawlikowski, M., Rizzi, N.L., 2016. Large deformations of planar extensible beams and pantographic lattices: Heuristic homogenization, experimental and numerical examples of equilibrium. Proc. R. Soc. A 472 (2185), 20150790. https://doi.org/10.1098/rspa.2015.0790.

dell'Isola, F., Seppecher, P., Alibert, J.J., Lekszycki, T., Grygoruk, R., Pawlikowski, M., Hild, F., 2018. Pantographic metamaterials: An example of mathematically driven design and of its technological challenges. Continuum Mech. Thermodyn. 31 (4), 851–884.

dell'Isola, F., Maier, G., Perego, U., Andreaus, U., Esposito, R., Forest, S., 2014. The complete works of Gabrio Piola: Volume I: Commented English Translation-English and Italian Edition. In: Advanced Structured Materials. Springer International Publishing, p. 813.

Egami, T., Fan, Y., Iwashita, T., 2017. Mechanical Deformation in Metallic Liquids and Glasses: From Atomic Bond-Breaking to Avalanches. In: Avalanches in Functional Materials and Geophysics. Springer, pp. 199–225.

Eremeyev, V.A., Pietraszkiewicz, W., 2016. Material symmetry group and constitutive equations of micropolar anisotropic elastic solids. Math. Mech. Solids 21 (2), 210–221.

Eugster, S.R., dell'Isola, F., 2017. *Exegesis of the Introduction and Sect. I from "Fundamentals of the Mechanics of Continua"*** by E. Hellinger.* ZAMM-Journal of Applied Mathematics and Mechanics/Zeitschrift für. Angewandte Mathematik und Mechanik 97 (4), 477–506.

Frenzel, T., Kadic, M., Wegener, M., 2017. Three-dimensional mechanical metamaterials with a twist. Science 358 (6366), 1072–1074.

Giorgio, I., Rizzi, N., Turco, E., 2017. Continuum modelling of pantographic sheets for out-of-plane bifurcation and vibrational analysis. Proc. Royal Soc. A: Math. Phys. Eng. Sci. 473 (2207), 20170636.

Goda, I., Assidi, M., Ganghoffer, J., 2012. Cosserat 3D anisotropic models of trabecular bone from the homogenisation of the trabecular structure. Comput. Methods Biomech. Biomed. Eng. 15 (sup1), 288–290.

Ha, C.S., Plesha, M.E., Lakes, R.S., 2016. Chiral three-dimensional isotropic lattices with negative Poisson's ratio. Physica Status Solidi (b) 253 (7), 1243–1251.

Lakes, R., 2001. Elastic and viscoelastic behavior of chiral materials. Int. J. Mech. Sci. 43 (7), 1579–1589.

Lemaître, A., Maloney, C., 2006. Sum rules for the quasi-static and visco-elastic response of disordered solids at zero temperature. J. Stat. Phys. 123 (2), 415.

Liu, X., Hu, G., 2016. Elastic metamaterials making use of chirality: A review. Strojniški vestnik-J. Mech. Eng. 62 (7–8), 403–418.

Misra, A., 1998. Particle kinematics in Sheared Rod Assemblies. In: Physics of Dry Granular Media. Springer, pp. 261–266.

Misra, A., Jiang, H., 1997. Measured kinematic fields in the biaxial shear of granular materials. Comput. Geotech. 20 (3–4), 267–285.

Misra, Anil, Placidi, Luca, Turco, Emilio, 2018. Variational Methods for Discrete Models of Granular Materials. In: Altenbach, Holm, Öchsner, Andreas (Eds.), Encyclopedia of Continuum Mechanics. Springer Berlin Heidelberg, Berlin, Heidelberg, pp. 1–14. https://doi.org/10.1007/978-3-662-53605-6_172-1.

Misra, A., Poorsolhjouy, P., 2015. Identification of higher-order elastic constants for grain assemblies based upon granular micromechanics. Math. Mech. Complex Syst. 3 (3), 285–308.

Misra, A., Poorsolhjouy, P., 2016. Elastic behavior of 2D grain packing modeled as micromorphic media based on granular micromechanics. J. Eng. Mech. 143 (1), C4016005.

Misra, A., Poorsolhjouy, P., 2016. Granular micromechanics based micromorphic model predicts frequency band gaps. Continuum Mech. Thermodyn. 28 (1–2), 215–234.

Misra, A., Nejadsadeghi, N., De Angelo, M., Placidi, L., 2020. Chiral metamaterial predicted by granular micromechanics: Verified with 1D example synthesized using additive manufacturing. Continuum Mech. Thermodyn. https://doi.org/10.1007/s00161-020-00862-8.

Misra, A., Poorsolhjouy, P., 2017. Grain- and macro-scale kinematics for granular micromechanics based small deformation micromorphic continuum model. Mech. Res. Commun. 81, 1–6.

Nejadsadeghi, N., Misra, A., 2019. Extended granular micromechanics approach: A micromorphic theory of degree n. Math. Mech. Solids. https://doi.org/10.1177/1081286519879479.

Poncelet, M., Somera, A., Morel, C., Jailin, C., Auffray, N., 2018. An experimental evidence of the failure of Cauchy elasticity for the overall modeling of a non-centro-symmetric lattice under static loading. Int. J. Solids Struct. 147, 223–237.

Poorsolhjouy, P., Misra, A., 2019. Granular micromechanics based continuum model for grain rotations and grain rotation waves. J. Mech. Phys. Solids 129, 244–260.

Reasa, D.R., Lakes, R.S., 2019. Cosserat effects in achiral and chiral cubic lattices. J. Appl. Mech., 86(11)

Richefeu, V., Combe, G., Viggiani, G., 2012. An experimental assessment of displacement fluctuations in a 2D granular material subjected to shear. Geotechnique Lett. 2, 113–118.
Seppecher, P., Alibert, J.-J., dell'Isola, F., 2011. Linear elastic trusses leading to continua with exotic mechanical interactions. J. Phys. Conf. Ser. 319, (1) 012018.
Spagnuolo, M., Peyre, P., Dupuy, C., 2019. Phenomenological aspects of quasi-perfect pivots in metallic pantographic structures. Mech. Res. Commun. 101, 103415.
Spencer, A.J.M., 2004. Continuum Mechanics. Courier Corporation.
Turco, E., Misra, A., Pawlikowski, M., Dell'Isola, F., Hild, F., 2018. Enhanced Piola-Hencky discrete models for pantographic sheets with pivots without deformation energy: Numerics and experiments. Int. J. Solids Struct.
Turco, E., dell'Isola, F., Misra, A., 2019. A nonlinear Lagrangian particle model for grains assemblies including grain relative rotations. Int. J. Numer. Anal. Meth. Geomech. 43 (5), 1051–1079.
Wang, D., 2018. Response of Granular Materials to Shear: Origins of Shear Jamming, Particle Dynamics, and Effects of Particle Properties. Duke University.